Shahrekord University

Journal of Microfluidic and Nanofluidic Research

Journal homepage: https://jmnr.sku.ac.ir

JMNR

Research Article

Determination of Effective Parameters on Wavy Microchannel Heatsink Performance after Adding Microtubes Using Response Surface Methodology

Akram Jahanbakhshi [a], Afshin Ahmadi Nadooshan [b*]

[a] *Department of Mechanical Engineering, Shahrekord University, Shahrekord, Iran*

[b] *Department of Mechanical Engineering, Shahrekord University, Shahrekord, Iran*

ARTICLE INFO

Article history:
Received: 2024-06-19
Revised: 2025-07-27
Accepted: 2025-07-28

Keywords:
MCHS;
Numerical modeling;
Response surface (RSM);
Wavy microtube;
Nanofluid;

ABSTRACT

In the present study, after doing some numerical modeling of the problem with the finite volume method (FVM) and specifying the effective parameters, by extracting a mathematical response surface (RSM), the effect of adding a microtube on the thermal and hydrodynamic performance of a wavy micro heatsink (MCHS) is investigated. The interaction between the input parameters of the problem, which are the geometrical variables of the microtube and their effect on the output parameters such as total heat transfer coefficient (h), total pumping power, total thermal resistance, entropy generation (S_{gen}), etc. are evaluated by an RSM statistical model. In the present study, the microtube and the microchannel are considered simultaneously in a wavy MCHS, and the new geometry of MCHS for cooling Central processing units (CPU) is presented. The results show that increasing Reynolds number (Re) and nanoparticle concentration (ϕ) in all studied geometries improves MCHS performance and reduces CPU surface temperature as well as thermal and total irreversibility rate and causes temperature uniformity; however, increasing the Reynolds number has a negative effect on the pumping power of the system. Then, the solution of the genetic iterative algorithm was used to find the best type of Response Surface for each output parameter. And then, the accuracy of mathematical models made by RSM for objective functions was proved. It is found that the accuracy of the Response Surface of the temperature uniformity on the CPU surface has a very high error, and as a result, this Response Surface does not provide a good estimate. Also, the response surface performs better in the estimation of frictional and thermal sgen. One of the results of the MCHS analysis based on RSM is that the distance of the microtube from the bottom of the MCHS does not affect pumping power. However, changing the mass fraction, Re, and microtube diameter changes the pumping power.

1. Introduction

In recent years, the construction of tools on a very small scale has led to extensive scientific research in the field of microfluidics and microelectromechanical systems. Microsystems are used in various fields of engineering, such as biological therapies in medicine, chemical analysis, cooling of electronic devices, separating reactors for biological cells, etc. Today, the use of microsystems is growing rapidly. Meanwhile, with the development of small-scale electronics industries, the issue of high heat generation per unit volume surface in electronic microchips is considered due to high density.

*** Corresponding author.**
E-mail address: *ahmadi@sku.ac.ir*

Cite this article as:

Jahanbakhshi, A. and Ahmadi Nadooshan, A., 2025. Determination of Effective Parameters on Wavy Microchannel Heatsink Performance after Adding Microtubes Using Response Surface Methodology. *Journal of Microfluidic and Nanofluidic Research*, 2(3), pp. 134-150. https://doi.org/10.22034/jmnr.2026.116645

A microchip consists of an integrated set of mechanical components, sensors, and electronic circuits so that all the components are placed inside a small device. Micro channels and micro pumps are the essential components of such systems. A microchannel is a large number of channels with micro dimensions and a characteristic length between 1 and 100 micrometers, which are placed on the electrically passive surface of the microprocessor and are used to dissipate the emitted heat. Microchannel is a useful practical solution for heat rejection due to its many advantages such as small geometric dimensions, high surface-to-volume ratio, high thermal conductivity in the solid part, and the need for small volumes of coolant [1-2].

MCHSs were first proposed by Tuckerman and Pease in 1981. Air, water, ethylene glycol, and engine oil are commonly used as refrigerants in MCHS. In general, two methods are used to increase the thermal performance of MCHSs. The first method is to change the microchannel geometry. In the second method, a working fluid with more suitable physical properties can be used or the physical properties of the fluid can be modified. Hu et al. [4] examined the thermal performance of forced convection of copper microchannel using aluminum oxide/water nanofluid as a coolant. He concluded that the use of nanofluids in MCHSs significantly increases the overall value of h. Chen and Ding [5] investigated heat transfer in microchannels containing aluminum oxide/water nanofluids, concluded that changes in temperature distribution and thermal resistance are significantly greater than thermal inertia. Winodhan and Rajan [6] investigated the performance of an MCHS with rectangular microchannels by considering water as a cooling fluid numerically. They considered the four arrangements A, B, C, and D with different inlets and outlet streams. They showed that for constant heat flux, the four arrangements performed better in terms of thermal resistance and Nusselt number than conventional arrangement. Fanny et al. [7] evaluated the forced convection heat transfer of a laminar flow of water-copper oxide/water nanofluid in a trapezoidal MCHS. They considered Brownian motion and used the two-phase method and showed that the Brownian diffusion increases by increasing temperature and ϕ, but decreases with the diameter of nanoparticles.

Kalteh and Abedinzadeh [8] by a numerical study of flow and heat transfer of water/aluminum nanofluid in a two-dimensional microchannel under the effect of the magnetic field, concluded that by increasing Re from 5 to 25 and increasing ϕ from 0 to 4%, heat transfer performance increases by 19% and 17%, respectively. They also stated that with increasing Hartmann number (Ha), the average Nusselt number (Nu_{av}) increases. For example, at Re = 25, increasing Ha from 0 to 10 results in Nu_{av} increases approximately 3%.

Lin et al. [9] used a numerical method to design an MCHS with wavy channels. They proposed the most suitable geometry in terms of cooling power by fixing the pumping power of the system and changing the wavelength and frequency of the channels. The results showed that with increasing amplitude and decreasing wavelength, the performance of thermal MCHS significantly improves. Rostami et al. [10] evaluated heat transfer in a wavy microchannel and optimized the microchannel geometry to obtain the maximum Nu. In this research, a constant heat flux boundary condition has been applied on the bottom wall and water is selected as the working fluid. Also, the body material of the silicon microchannel is considered. They concluded that the geometric parameters affect the intensity of the secondary currents and the magnitude of the fluid circulation area. Their results also showed that there is an optimal state for Nu for the wavy microchannel. Khorasanizadeh et al. [11] examined the operation of an MCHS consisting of seven microchannels with an isosceles triangle cross section numerically. They examined the I-shaped arrangement with horizontal entry and exit and the U-shaped one with vertical entry and exit. They found that the thermal performance of a heat well depends on the shape and geometry of the microchannel in addition to the arrangement of the inlet and outlet. A new design of an MCHS was proposed by Ahmed et al. [12]. Their results revealed that the triangular microchannel with two-layer channels has a 27.4% decrease in wall temperature compared to the two-layer rectangular one. Ghasemi et al. [13] evaluated the mixed heat transfer of alumina/water nanofluid in an MCHS with a triangular microchannel. Increasing ϕ enhances h and decreases the thermal resistance. Tefraji et al. [14] demonstrated that a trained network can be used as a suitable method to perform experiments in the microchannel. Ali and Ershad [15] examined the impact of pin angle on the performance of microchannels and revealed that the microchannel with an angle of 22.5° has the lowest thermal resistance. Peighambarzadeh et al. [16] evaluated the efficiency of water-aluminum oxide and water-copper oxide nanofluids in a rectangular heat absorber microchannel. They concluded that water-copper oxide nanofluid (ϕ = 0.2%) and water-oxide nanofluid (ϕ = 1%) increase *h* by 27% and

49%, respectively. Gol et al. [17] numerically investigated the mixed convective heat transfer and s_{gen} for aluminum/water nanofluid in a three-dimensional microchannel. They reported an enhancement in h by intensifying the magnetic field. They also reported a decrease in total s_{gen} by increasing ϕ, channel aspect ratio, and magnetic field. Some of their results are not in agreement with the scientific predictions, indicating that the issue needs further investigations. Wang and Hu [18] investigated the existence of a cylindrical block for pressure-driven flow within a Y-shaped microchannel experimentally and numerically. They evaluated the effect of parameters such as block diameter, its location, and number at different values of Re to increase the mixing efficiency. They showed that the presence of a block increases lateral convection and improves mixing. Sarlak et al. [19] revealed that the use of nanofluids containing carbon nanotubes reduces the overall thermal resistance of two-layer MCHS compared to nanofluids containing metal oxides that have Newtonian rheological behavior. Haj Mohammadi et al. [20] investigated the microfluidic effects on increasing heat transfer and the optimal design of an MCHS. The purpose of this study was to present an optimal geometric structure of an MCHS, assuming a slip boundary condition. It was reported that the channel aspect ratio increases as the slip parameter increases. Al-Rashed et al. [21] evaluated the use of water-silver nanofluid in a corrugated MCHS. They investigated the effect of adding nanofluid to the system at different values of Re and obtained the most efficient values for the wavy channel by examining different geometric parameters for the microchannel. Azizi et al. [22] considered convection heat transfer in a cylindrical MCHS and concluded that h of nanofluid has a significant increase compared to the base fluid and increasing Re leads to a decrease in thermal performance. Subasi et al. [23] performed multi-objective optimization of a honeycomb MCHS using the response surface methodology. Their study aimed to find the optimal values of design parameters of an MCHS with hexagonal aluminum honeycomb fins by employing the response surface methodology (RSM) and Pareto-based multi-objective optimization. The geometric characteristics of the fin, the angle of attack, and Re were selected as design variables and Nu and friction coefficient were selected as the objective function. It was concluded that the resulting set of Pareto solutions provides an important insight into the design parameters and allows designers to choose within the optimal range.

RSM estimates the correlation between response variables and independent ones [24-25]. Using the RSM, fewer experiments or numerical modeling are required. In the present study, the optimal geometry introduced by Al-Rashed et al. [21] is used as the reference geometry. The mathematical response is determined to investigate the effect of microchannels and corrugated microtubes on the MCHS. One of the innovations of the present study is the simultaneous existence of two geometries of microtube and microchannel in a wavy MCHS. In addition to the geometry, the choice of working fluid in the MCHS is also important. Therefore, water-ethylene glycol 50%/silver nanofluid is considered to improve the performance of MCHS. Since in this study we are looking for a way to get the most out of the results from the data obtained from a certain number of direct numerical simulations, the RSM was chosen to construct the required mathematical models and analysis of the desired wavy MCHS. In addition, data analysis can also be performed simultaneously by optimizing the output variable that is influenced by input variables. The effectiveness of RSM is evaluated in optimizing the structure of an MCHS with geometry involving a microtube

2. Description of the model

2.1. Geometry and boundary conditions

Fig. 1 shows the geometry of the MCHS. The MCHS has 50 wavy channels where a wavy tube is placed between the two microchannels

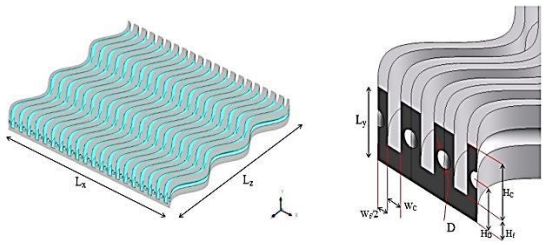

Fig. 1. The geometry of the problem

According to the studies of Al-Rashed et al. [21], the microchannel dimensions are fixed. In the present study, the diameter of the microtube, its distance from the bottom, and the flow ratio between the microtube and the microchannel are investigated. Due to the symmetry of the problem, only one strip containing a channel and two half-tubes are considered. The flow rate is also determined based on the nominal Re based on the microchannel hydraulic diameter and the mass-to-microchannel mass flow ratio (fr). Table 1 shows the dimensional parameters of the problem based on Fig. 1.

Table 1. Dimensional parameters of the problem.

Value	Parameter
10mm	LX
350μm	LY
15mm	LZ
120 μm	Wf
80 μm	WC
70~90 μm	D
100 μm	Hf
250 μm	HC
100~290 μm	HD
0.25~0.75	fr
150~1500	Re_n

It is assumed that the MCHS is mounted on a CPU, and 50 W/cm² heat flux is applied to the system from its bottom surface.

The geometry of the channel and tube along the MCHS is defined as follows:

$$S(z) = a_W \sin\frac{2\pi z}{L_W} \quad (1)$$

The value of the parameters a_W and a_W is based on the work of Al-Rashed et al. [21], who investigated an MCHS with a wavy microchannel. Based on this study, $a_W = 138\mu m$ and $L_W = 5mm$ lead to the maximum rate of heat transfer and PEC among the studied values. In the present study, the same geometry is used for channels and tubes.

2.2. Properties of nanofluid

Sarafraz and Hormozi [27] could synthesize silver nanoparticles from green tea leaves the nanoparticles were synthesized using an environmentally friendly process which is a clean method. In the present work, according to the information of these researchers, a mixture of water and 50% ethylene glycol is used as a base fluid and silver nanoparticles. The properties of the nanofluid mixture are calculated based on this research. Density, specific heat capacity, viscosity, and thermal conductivity of nanofluid are calculated based on the volume percentage of nanoparticles in the nanofluid using the following equations.

$$\rho_{nf} = (1-\phi)\rho_{bf} + \phi\rho_p \quad (2)$$

$$\rho_{nf}C_{p,nf} = (1-\phi)\rho_{bf}C_{p,bf} + \phi\rho_p C_{p,p} \quad (3)$$

$$\mu_{nf} = \mu_{bf}(1+2.5\phi) \quad (4)$$

$$k_{nf} = k_{bf}[0.981 + 0.00114T(°C) + 30.661\phi \quad (5)$$

where ρ is the density, C_p specific heat capacity, μ viscosity, k thermal conductivity, and T temperature

2.3. Governing equations

In this study, the flow is in the laminar flow regime. The simulations are performed by solving the mass, momentum, and energy equations for the fluid region and the energy equation for the solid region. These equations are as follows [21]:

Continuity equation

$$\nabla.(\rho_{nf}\vec{u}) = 0 \quad (6)$$

Momentum equation:

$$\nabla.\left(\rho_{nf}\vec{u}\vec{u}\right) = -\nabla p + \nabla.(\mu_{nf}\nabla\vec{u}) \quad (7)$$

Energy equation for the fluid region:

$$\nabla.\left(\rho_{nf}\vec{u}C_{p,nf}T\right) = \nabla.(k_{nf}\nabla T) \quad (8)$$

Energy equation for rigid part:

$$\nabla.(k_s\nabla T) = 0 \quad (9)$$

where $\vec{u}$ is velocity vector and p the pressure. The s subscript refers to the properties of the solid.

2.4. Definition of analytical parameters

The parameter θ, as defined in Eq.10, describes the CPU surface temperature uniformity being cooled by the MCHS. Thus, the lower the value of this parameter, the more uniform the surface temperature of the processor relative to the heat flux. σ (T) presents another description of the temperature uniformity on the CPU surface

$$\theta = \frac{T_{CPU,Max} - T_{CPU,min}}{T_{CPU,Mean}} \quad (10)$$

$$\sigma(T) = \sqrt{\int\left(T - T_{CPU,Mean}\right)^2 dA} \quad (11)$$

In this equation, the maximum CPU surface temperature is expressed by $T_{CPU,Max}$, the minimum temperature is expressed by $T_{CPU,min}$ and the average CPU surface temperature is expressed by $T_{CPU,Mean}$.

The overall heat transfer coefficient of the MCHS is defined as follows, considering that its entire cooling performance is performed by the convection process.

$$h = \frac{q''}{T_{CPU,Mean} - T_{in}} \quad (12)$$

The amount of pumping power required for the MCHS is calculated using Eq. 13 based on the

volume flow and internal pressure drop of the MCHS

$$W_{pump} = \dot{V}\Delta p \tag{13}$$

In order to analyze the overall performance of the nanofluid in the MCHS, the term PEC is defined as follows:

$$PEC = \frac{h_{nf}/h_{bf}}{\Delta p_{nf}/\Delta p_{bf}} \tag{14}$$

The rate of sgen in integral form is obtained because the integral method is more accurate and its calculations are less sensitive to geometric meshing [27]:

Total sgen includes the thermal sgen of the fluid in the whole computational region (fluid and solid), sgen due to heat flux and frictional sgen, which are:

$$\begin{aligned}
&\dot{S}_{gen} = \dot{S}_h + \dot{S}_\mu - \dot{S}_q \\
&\dot{S}_h = \dot{m}\int_{in}^{out} c_p \frac{dT}{T} \\
&\dot{S}_\mu = \dot{m}\int_{out}^{in} \frac{v}{T} dP \\
&\dot{S}_q = \oint_A \frac{dQ}{T}
\end{aligned} \tag{15}$$

Considering the use of numerical solution and multi-input and multi-output in geometry, these equations have been calculated in the following form**:**

$$\begin{aligned}
\dot{S}_h &= \sum_{outlets} \iint_{S_{outlet}} \rho V C_p Ln\, T\, dA \\
&\quad - \sum_{inlets} \iint_{S_{inlet}} \rho V C_p Ln\, T\, dA \\
\dot{S}_\mu &= \sum_{inlets} \iint_{S_{inlet}} \frac{VP}{T}\, dA \\
&\quad - \sum_{outlets} \iint_{S_{outlet}} \frac{VP}{T}\, dA \\
\dot{S}_q &= \oint_A \frac{q''}{T} dA
\end{aligned} \tag{16}$$

2.5. Numerical solution process

ANSYS FLUENT 18.0 software is used to solve the governing equations. The second-order UPWIND method is used to solve the momentum equation and the SIMPLE method with a staggered pressure grid is employed for the velocity and pressure field coupling. The convergence criterion is set to 10-8 for the energy equation and 10-6 for the other equations based on the scaled residual.

In the present study, only one channel is modeled using the symmetry boundary condition. The modeled geometry for the two states without microtube and including microtube is shown in Figure 2.

In modeling of MCHS without microtube, there are two computational zones and in the case of microtube, there are four computational zones, one of which is the solid part of the MCHS body in which only the temperature equation is solved and the other areas are fluid and flow equations. And the energy in them is solved numerically

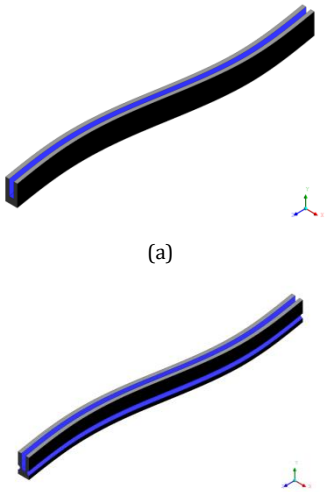

(a)

(b)

Fig. 2. MCHS with two different geometries: (a) without microtube, (b) with microtube.

2.6. Boundary conditions

2.6.1 Boundary condition of inlet

$$\begin{aligned}
&\dot{m}_{total} = \frac{\pi}{4} Re_n\, D_h\, \mu \\
&\dot{m}_{Pipe} = fr \times \dot{m}_{total} \\
&\dot{m}_{Channel} = (1 - fr)\dot{m}_{total}
\end{aligned} \tag{17}$$

$$Re = \frac{\rho u D_h}{\mu} \tag{18}$$

Here, D_h is a “characteristic width” of the channel, defined as

D_h=4. (cross-sectional area)÷(perimeter p).

In the numerical modeling process for the fluid-solid interface, the velocity components are zero on these walls, and the pressure gradient perpendicular to the plane is zero, and also in the equation of temperature energy and heat flux between the flow and the inner wall of the solid region are equal to:

$$\begin{aligned}
&\frac{\partial \overrightarrow{P_n}}{\partial \vec{n}} = 0 \\
&\left.\frac{\partial T}{\partial \vec{n}}\right|_{solid} = \left.\frac{\partial T}{\partial \vec{n}}\right|_{Fluid}
\end{aligned} \tag{19}$$

$$T|_{solid} = T|_{Fluid} \quad (20)$$

the outflow surfaces zone has a relative static pressure of zero (absolute one atmosphere). The components of velocity and temperature in the governing equations are calculated based on the SIMPLE algorithm, the general form of which is in the form of relation (21)

$$u_{I,j,k} = u^*_{I,j,k} + d_{I,j,k}\left(P^*_{I,j,k} - P^*_{I-1,j,k}\right) \quad (21)$$

Thermal symmetry is considered for the solid zone wall, which, based on the iterative pattern of the thermal well, separates a strip consisting of a microchannel and two half microtubes, in which only the temperature equation will be solved. At this level, the gradient perpendicular to the plane is zero

$$\left.\frac{\partial T}{\partial \vec{n}}\right|_{solid} = 0 \quad (22)$$

The independence of the grid is investigated for channels and tubes (Table 2). For this purpose, the Re of channel and tube is 700 and 70, respectively, and ϕ = 0.1%.

Table 2. Results of the grid-independence test.

No. of elements	ΔT [K]	W_{pump} [W]
24000	3.386	0.0186
27000	3.387	0.0475
74000	3.388	0.0568
128000	3.388	0.0587
195000	3.388	0.0591
330000	3.388	0.0591

According to Table 2, the grid with 195000 elements is selected as the computational grid for further simulations in geometry includes microtube and microchannel which are shown in Figure 3.

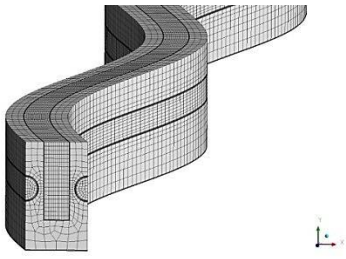

Fig. 3. A schematic view of the computational grid.

To validate the modeling, the present work is compared with the experimental results of Sui et al. [28]. Based on this paper, a wavy microchannel is modeled according to the parameters of Table 3. A comparison between the overall Nusselt number calculated by numerical solution with the experimental results of reference [28] is shown in Fig. 4. The maximum difference between the present results and the experimental ones is 8%, which is related to Re = 300. There is also a 3% error for Re = 500. For Re = 700, the result of the present work is completely in agreement with the experimental one of reference [28].

Table 3. Dimensional parameters of the validation case.

Value	Parameter
193 μm	Wf
207 μm	WC
100 μm	Hf
406 μm	HC
138 μm	aW
25 mm	LZ

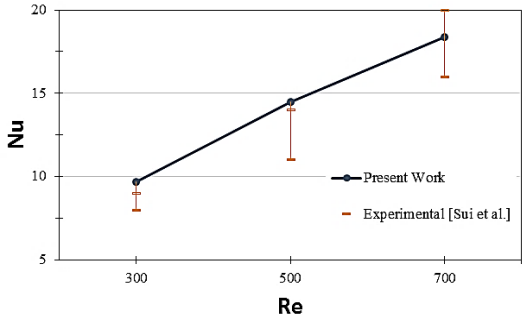

Fig. 4. Validation of the present work with the one reported by Sui et al. [29].

3. Response surface method (RSM)

RSM uses experimental design and regression analysis to establish an appropriate operating correlation between the desired response (y), and independent input variables that affect the system response (xi, xj). In this research, a second-order polynomial model is considered and the final result is the weighted result of these response surfaces as follows:

$$y_n = w_{n,1}y_{n,1} + w_{n,2}y_{n,2} + w_{n,3}y_{n,3} \quad (23)$$

where $y_{n,i}$ represents one of the expressed response surfaces and $w_{n,i}$ is its weight coefficient. The sum of these weight coefficients is equal to one. y_n is the prediction of the ensemble

$$\sum_{i=1}^{m} w_i = 1 \ \ and \ w_i \geq 1 \ , \quad 1 \leq i \leq m \quad (24)$$

$$y_{n,1} = \sum^{m} a_i x_i + \sum_{i=1}^{m}\sum_{j=1}^{m} b_{ij} x_j x_i \quad (25)$$

where x_i and x_j are input variables and m represents their number ($m \geq 1$). $y_{n,1}$ is the nth output variable, which is estimated by the method of complete polynomial equations. The coefficients a_i and b_{ij} are unknown parameters of the model (the tuning parameters). In this method, the difference between the output

parameters and the estimated value of the function is compared as follows:

$$SSE = \sum_{all\ train\ points} \left(y_{n,1} - \hat{y}_{n,1}\right)^2 \quad (26)$$

where $y_{n,1}$ is the real value of the output parameter and $\hat{y}_{n,1}$ is the estimated value of the function. By minimizing the SSE value, the response surface function is determined.

The estimation of the value of the nth output parameter by the non-parametric regression method is as follows

$$y_{n,2} = \sum_{i=1}^{m} < W, \boldsymbol{X} > + b \quad (27)$$

where X is the vector of input variables, W is the vector of unknown coefficients and b is the unknown constant parameter. < > shows dot product. $y_{n,2}$ represents the estimation of the output parameter using the non-parametric regression method.

In this method, the following procedure is done to find the values of W and b. First, the equation is written using the Kronecker function (Eq. 28) where A_i^* and A_i are Lagrangian coefficients

$$y_{n,2} = \sum_{i=1}^{m} (A_i - A_i^*) K(\boldsymbol{X}_i, \boldsymbol{X}) + b \quad (28)$$

Defining the error tolerance value ϵ and finding the values that minimize the sum of the error in the estimation equation leads to the following optimization form:

$$MIN_{A,A^*}\ 0.5 \sum_{i=1}^{m}\sum_{j=1}^{m}(A_i - A_i^*)(A_j - A_j^*)K(\boldsymbol{X}_i, \boldsymbol{X}_j) + \sum_{i=1}^{m}[\epsilon(A_i + A_i^*) - y_i(A_i - A_i^*)] \quad (29)$$

$$S.T.\ 0 < A_i < C\ \&\ \sum_{i=1}^{m}(A_i - A_i^*) = 0$$

$$y_{n,3} = \sum_{i=1}^{m} a_i f_i(\boldsymbol{x}) + \sum_{i=1}^{m} \lambda_i r(x_i, \boldsymbol{x})$$

$$r(x_i, \boldsymbol{x}) = exp\left(-\sum_{k=1}^{m} \beta_k |x_k^i - x_k^j|^2\right) \quad (30)$$

where a_i, λ_i and β_k are unknown coefficients of the model. $f_i(x)$ is a polynomial function

4. Results and discussions

4.1. The results of CFD simulation

First, the hydraulic and thermal parameters of an MCHS with a microchannel containing silver/water-ethylene glycol 50% nanofluid with wavy channels are investigated to cool digital processors. The effect of wavy microtubes on the performance of the mentioned MCHS is also investigated. The modeling is based on ϕ = 0, 0.1%, 0.5%, and 1%, the presence and absence of wavy microtubes, and Re = 300, 500, 700, 1000, and 1500.

Fig. 5 shows h at different values of Re and ϕ for two cases with and without microtubes. The dashed lines are for the case without microtube and the solid lines are for the one with microtube. This figure shows that increasing ϕ enhances h. On the other hand, the higher Re, the greater the effect of increasing ϕ.

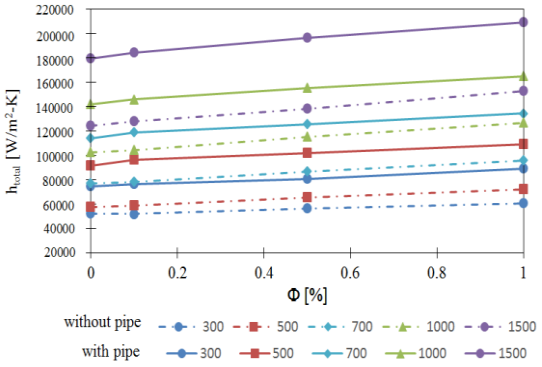

Fig. 5. The overall value of h.

It is demonstrated that the addition of microtubes causes a significant increase in the overall thermal coefficient of the system so that h for the system with microtubes is 80% and 110% of that without microtubes at Re = 500 and 700, respectively. The presence of microtubes increases the heat transfer between the body and the fluid. On the other hand, the presence of microtubes and the creation of more temperature mixing in the fluid flow causes the fluid temperature along with the channel to increase slightly. Thus, the temperature difference between fluid and solid is kept constant, leading to an increase in the heat transfer rate. The effect of increasing nanoparticles and microtubes can also be investigated based on the average temperature and maximum temperature of the processor surface. As ϕ increases and the heat transfer performance in the system improves, the surface temperature of the processor decreases due to a lower temperature gradient (Fig. 6). This figure shows the decreasing trend of the average surface temperature due to the increase of ϕ. It is observed that the effect of nanoparticles is higher at low values of Re. Increasing ϕ at lower

amounts of Re causes the surface temperature of the processor to change more. On the other hand, the presence of microtubes has a much stronger effect.

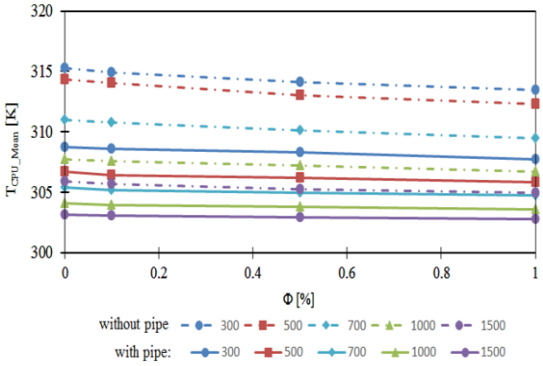

Fig. 6. Average CPU surface temperature.

For example, in the absence of microtubes, at Re = 300, the average temperature is 315 (K), but the addition of microtubes reduces this temperature to 309 K. The addition of 1% nanoparticles reduces the temperature by 2 degrees.

In addition to the average CPU surface temperature, the maximum CPU surface temperature and its temperature uniformity are important, because an excessive increase of CPU temperature and a low temperature difference in it have a negative impact on the performance of the processor. To investigate this point, the variation of the maximum surface temperature is given in Fig. 7.

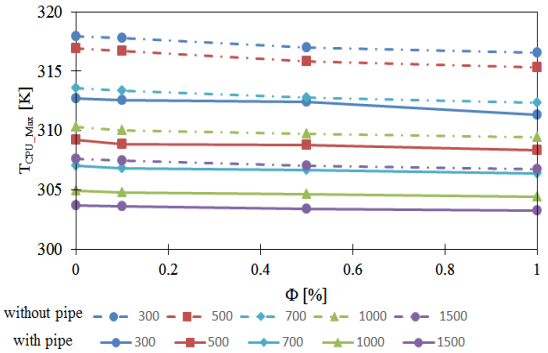

Fig. 7. Maximum CPU surface temperature.

Figs. 6 and 7 reveal that the average processor surface temperature is 308 K for the case without microtube at Re = 1000, while the maximum surface temperature is 310 K. This difference is due to the non-uniform heat transfer at the processor surface because the heat transfer conditions and heat resistance of all points on the processor surface are not the same, resulting in a temperature difference on the surface. The presence of nanofluids improves cooling performance and reduces the maximum temperature. At the same time, the presence of microtubes causes the amount of average and maximum temperature difference at the CPU level to be greatly reduced due to the increase in the heat transfer of the system and reduction in the thermal resistance of further parts of the processor.

The more uniform the temperature inside the channel, the better the mixing of the flow and the better its thermal performance. Fig. 8 shows the nanofluid temperature contours in the output region. For all cases, the wall is hotter than the central part, but the temperature of the central part remains unchanged. The effect of increasing nanoparticles on the temperature distribution from the walls to the center is not recognizable.

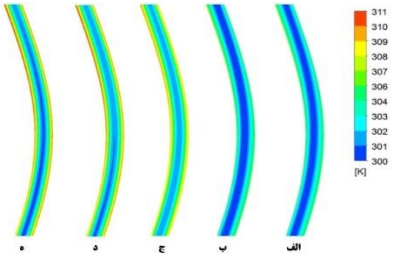

Fig. 8. Temperature distribution in a rectangular channel: a) Re = 700, φ = 1%, b) Re = 700, φ = 0.1%, c) Re = 300, φ = 1%, d) Re = 300, φ = 0.5%, and e) Re = 300, φ = 0.1%.

This is due to the high velocity and strong convection heat transfer in the flow direction compared to the conductive heat transfer in the direction perpendicular to the flow. In Figs. 8c, d, and e, which are related to Re = 300, the heat dissipation in the direction perpendicular to the flow occurs better due to the lower convection heat transfer. The increase of nanoparticles enhances this phenomenon so that the temperature changes reach the flow center. To reach the temperature at the central core of the flow, a temperature gradient is needed perpendicular to the flow direction. This means that the temperature of the fluid at the wall increases, which reduces h between the fluid and the solid and increases the temperature of the solid surface to transfer heat flux. Fig. 9 shows that the heat transfer in the vertical direction is much stronger due to the smaller cross section. As a result, much more temperature changes are observed.

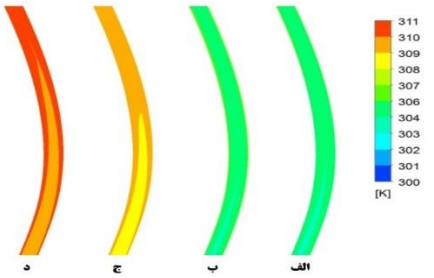

Fig. 9. Temperature distribution in the microtube: a) Re = 700, φ = 1%, b) Re = 700, φ = 0.1%, c) Re = 300, φ = 1%, d) Re = 300, φ = 0.1%.

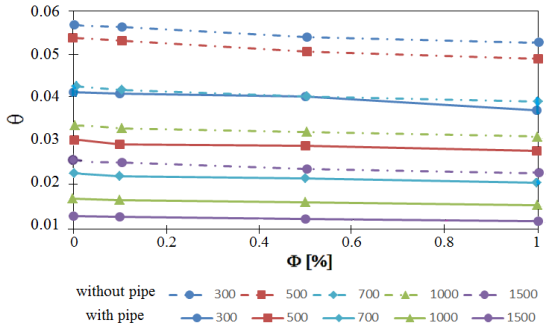

Fig. 10. Temperature uniformity.

Fig. 10 shows the ratio of the temperature range to the average temperature of the CPU surface. The smaller values of this number mean more uniformity of the temperature distribution on the CPU surface. Due to the increase in h due to the addition of nanofluid, the improvement of the thermal performance of the system is clear. It is also observed that the temperature becomes more uniform on the surface, but there is an inverse relationship between the effect of ϕ and Re. As Re increases, the distribution of temperature becomes more uniform due to the stronger convection heat transfer. As a result, the effect of increasing ϕ will not be significant. On the other hand, the creation of microtubes causes a more uniform distribution of CPU surface temperature due to increasing the heat transfer surface and decreasing the thermal resistance of the processor. For example, the surface temperature distribution for a flow with a microtube at Re = 700 is more uniform than that without a microtube at Re = 1500. Fig. 11 shows the required pumping power for different cases. The improvement of heat transfer in an MCHS should not be at the expense of high pumping power. It is clear that the addition of microtubes greatly increases the pumping power so that the pumping capacity for the case without microtube at Re = 1500 is equal to that at Re = 300 in the absence of microtube.

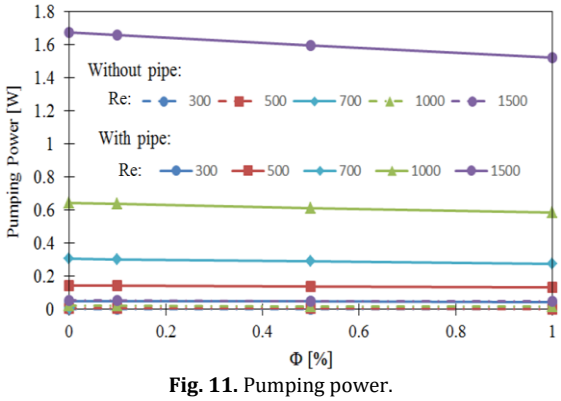

Fig. 11. Pumping power.

The required pumping power at Re = 700 is about six times Re = 1500 in the absence of a microtube. On the other hand, this figure shows that the addition of nanofluid reduces the pumping power. This phenomenon occurs due to the decrease in flow velocity due to the increase in fluid density when Re is kept constant.

For a general comparison between the improvement of thermal performance and the cost of pumping power, the PEC is defined to evaluate the thermal and hydraulic performance simultaneously. Different cases are compared in Fig. 12 by defining the base fluid as the reference case.

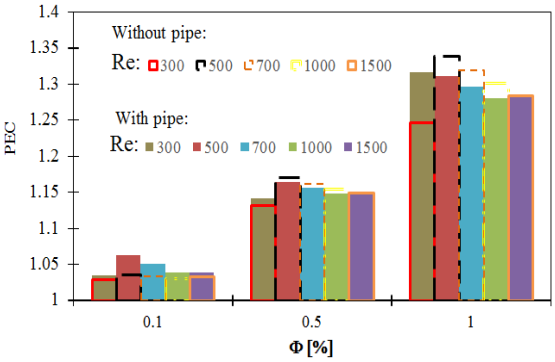

Fig. 12. PEC variations.

This figure shows that the addition of nanofluid does not have the same effect for different cases. So that a maximum performance improvement of 5% is obtained at ϕ = 0.1%. This performance improvement in the system is higher for the system with microtubes. But at ϕ = 0.5%, a maximum performance improvement of 15% is observed. At ϕ = 1%, there is a 35% improvement, while the addition of this concentration of nanoparticles in a system without a microtube improves the performance of the system. This is due to that the addition of nanoparticles improves the thermal diffusion of the fluid. For any case where the performance of the system depends on the thermal diffusion of the working fluid, the addition of nanoparticles improves the performance of the system.

In the following, sgen in the MCHS with microtubes is calculated using the integral method. Fig. 13 shows that regardless of ϕ in the fluid, increasing Re enhances frictional sgen. Fig. 14 shows the frictional sgen. It is found that the amount of frictional sgen has a second-order relationship with Re ($S_f \propto Re^2$). Also, the amount of frictional sgen decreases due to the increase of nanoparticles. It is directly related to ϕ and this relationship is independent of Re.

s_{gen} in terms of Re is shown in Fig. 15. It is revealed that the total sgen and the frictional sgen do not have the same trend so that the total sgen shows a third-order relationship with Re

($S_{gen} \propto Re^3$) and a specific behavior is not observed for the total sgen.

In this study, the equation for generating total sgen based on Re is equal to:

$$S_{gen} = (4E-12)Re^3 - (8E-09)Re^2 + (7E-06)Re - 0.0009 \quad (31)$$

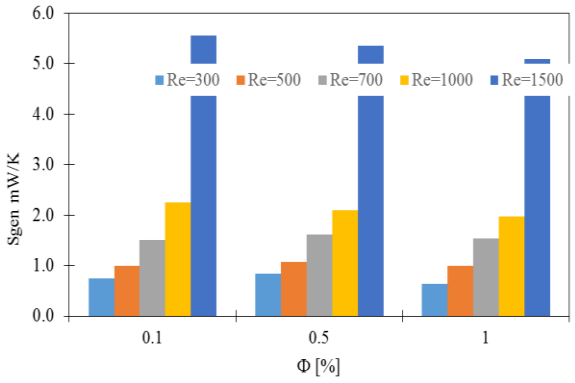

Fig. 13. Comparison of sgen in MCHS.

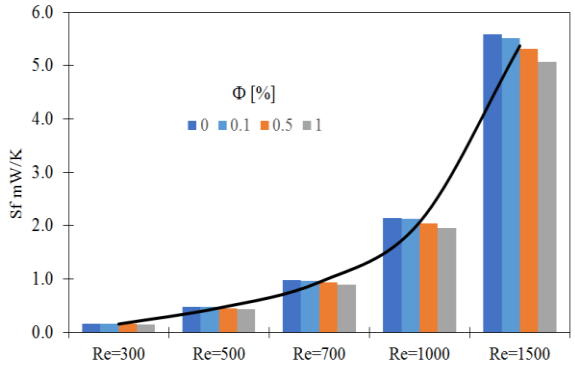

Fig. 14. Frictional sgen at different values of ϕ and Re.

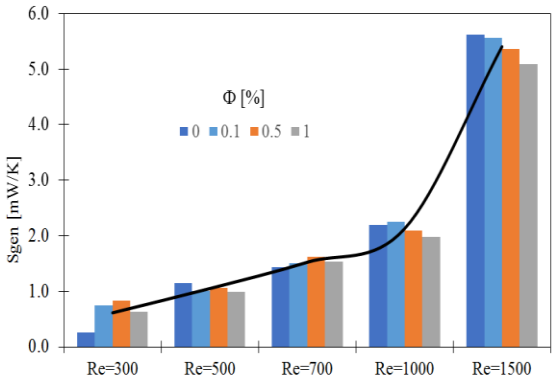

Fig. 15. sgen in terms of Re.

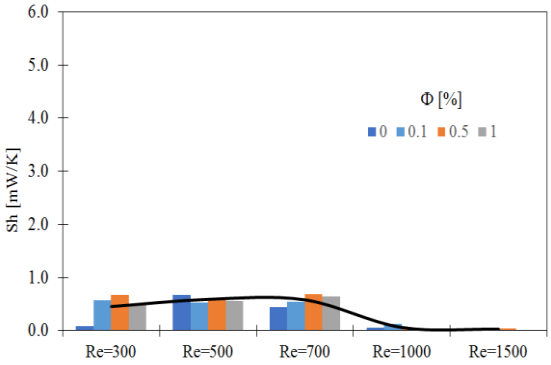

Fig. 16. Thermal sgen for different values of Re.

Fig. 16 shows the amount of thermal sgen. It is found that there is a decrease in the thermal sgen with Re due to an increase in the mass flow rate and a decrease in the temperature difference of the wall and fluid.

4.1.1 Minimum and maximum values of output parameters

In this section, the minimum and maximum values of output parameters such as average CPU surface temperature, total sgen, total pumping power, etc. based on the range of geometric parameters in this study and the values obtained based on numerical modeling are investigated and presented. In Table 4, the minimum and maximum output parameters and the equivalent values of their input parameters are presented. According to the parameters observed in this table, the ideal case for the MCHS is the minimum values of all parameters. As can be seen, all of these parameters do not have minimum values simultaneously. In general, the purpose of examining the minimum and maximum values of output parameters based on modeling is to determine the constraints of the problem and check the accuracy of the response surfaces

4.2. Study of MCHS based on RSM

In industrial processes, there are several input factors with different levels, each of which may affect the characteristics of the final product or system, and the response level methodology is used to analyze the issues in which the response variable is affected by several input variables. In the present study, an iterative genetic algorithm is used to obtain the most appropriate response level for each variable and output parameter [29].

4.2.1 Accuracy analysis of response surfaces

In addition to the input points to the response surface definition algorithm, six other modes are modeled separately which was used

to check the accuracy of these surfaces at points other than the initial points which are the same as the results of simulations. In this part of the research, output parameters such as microchannel mass flow rate, microtube mass flow rate, channel pressure drop, microtube pressure drop, mean hot surface temperature, maximum hot surface temperature, Re of microchannel and microtube, total pumping power, total thermal resistance, total entropy, thermal entropy, friction entropy, maximum microchannel outlet temperature, σ (T) and θ are considered and according to four inputs, i.e., design parameters including system flow rate, microtube to microchannel flow ratio, microtube diameter, and microtube distance from MCHS surface, response surface coefficients are obtained. In the following, the estimated accuracy of the obtained response surfaces is discussed and it is stated which parameters are reliable for the study. In Figs. 17 to 19, eight diagrams including output parameters are presented. in all the diagrams presented in this section, in the horizontal axis, the result obtained for the desired parameter from direct modeling, and in the vertical axis, the result obtained from the response surface are shown, and each amount the data points are closer to the line y = x, the response surface is more accurate. Figs. 17a and b show excellent accuracy of the results of the response surfaces for estimating the pressure drop.

Table 4. Minimum and maximum values of output parameters.

fr	H_D (μm)	Re_n	D (μm)	Minimum / Maximum	Parameter
0.25	100	150	90	3.55	Total pumping power (mW)
0.75	100	1500	70	4927	
0.63	243	1163	85	0.0000102	Total heat resistance $(\frac{K\,m^2}{W})$
0.75	196	150	90	0.0000778	
0.25	290	150	90	0.0000828	Total sgen (W/K)
0.75	290	1500	70	153	
0.25	217	669	90	0.33	$\sigma\,(T)$ (K)
0.34	218	204	70	60.26	
0.63	148	488	85	0.005	θ
0.34	218	204	70	0.067	
0.63	243	1163	85	305.11	Average surface temperatur CPU e of (K)
0.75	196	150	90	338.92	
0.38	243	1163	85	306.28	Maximum surface temperatur CPU e of (K)
0.75	196	150	90	340.57	

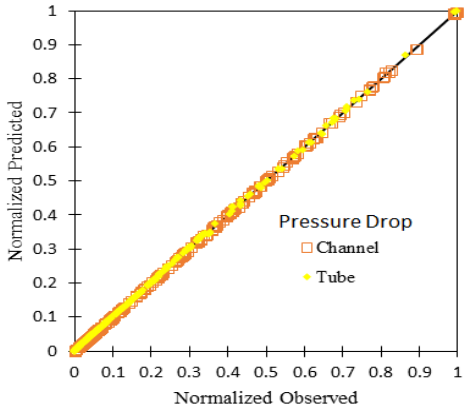

(a)

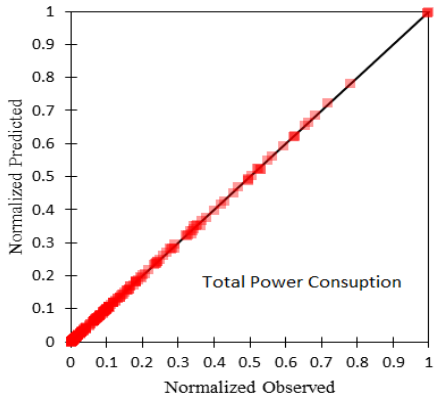

(b)

Fig. 17. Normalized values of response surfaces in terms of modeling values - Hydrodynamic parameters

The three diagrams in Fig. 18 show the accuracy of the results for the thermal parameters. Accuracy of response surfaces in estimating the maximum temperature on the CPU surface, especially at the maximum temperatures available seems to have a high error, but note that the green lines show the error range of 3%. Hence, response surfaces have less than 5% error to estimate the maximum CPU surface temperature in the worst cases. The average temperature estimate of this surface has a maximum error of 3%. The smaller the range of changes of a parameter in the range of input parameters, the more scatter appears in these figures.

In Fig. 18 b, the results of the accuracy of the response surfaces of the temperature uniformity parameters on the CPU surface are illustrated. The response surfaces have an error not only in the upper range of the graph but also in the lower range, which is the optimal range in the MCHS design. In this figure, the green lines show the error range of 20% and as a result, this response surface is not a good estimate for this parameter. Finally, Fig 18 c shows the accuracy of thermal resistance estimation, and the green

lines provide an error range of 10%, which in the lower 20% range provides acceptable estimations of thermal resistance values.

Fig. 19 shows the accuracy of estimating sgen. Fig. 19a states that the estimates of response surfaces for total sgen are acceptable in the model. But Fig. 19 b shows that these response surfaces perform better for the frictional sgen in the estimation of frictional and thermal sgen. In this figure, the green lines show the 10% error. It is preferred to use a combination of response surfaces of thermal sgen to frictional sgen ratio. According to the green lines in this figure, an error of 10% is observed for very high ratios.

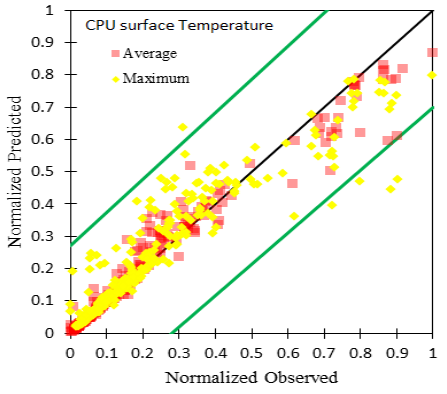

(a)

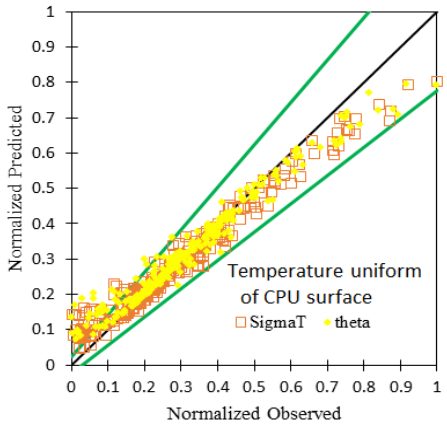

(b)

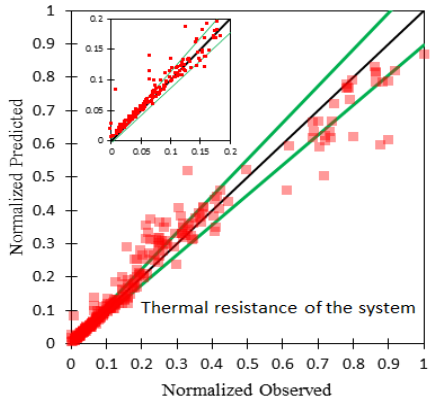

(c)

Fig. 18. Normalized values of response surfaces in terms of modeling values - thermal parameters.

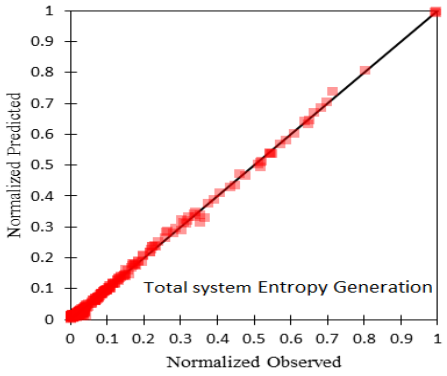

(a)

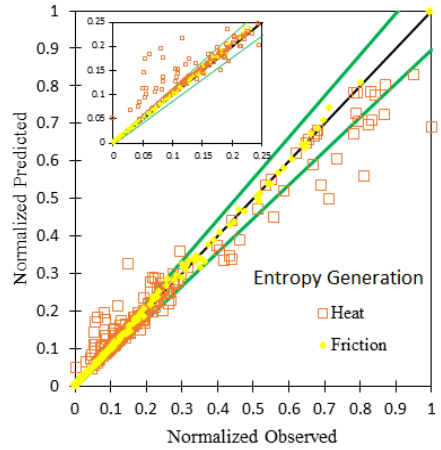

(b)

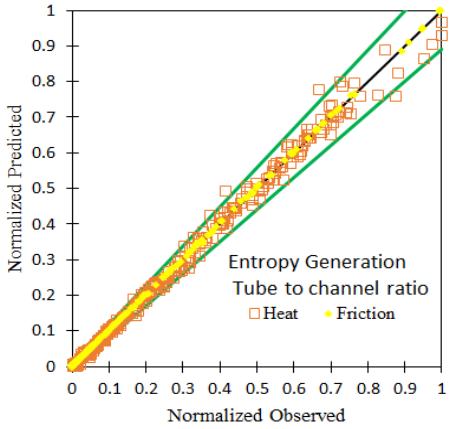

(c)

Fig. 19. Normalized values of response surfaces in terms of modeling values.

4.3. Analysis of RSM results

In this section, according to the obtained response surfaces, the MCHS behavior is analyzed based on the defined input parameters.

Fig. 20 shows the pumping power that the micro MCHS needs. Pumping power is a hydrodynamic parameter and the distance of the microtube from the bottom of the MCHS does not affect it. But changing the other three parameters, namely mass fraction, nominal Re, and microtube diameter change the pumping power. Comparing the two Figs. 19 a and b show that the mass fraction of the flow rate of the microtube is directly related to the increase of

pumping power. With increasing mass fraction, the pumping power required by the system is also increased. The nominal Re is also directly related to the pumping power. The reason is that the fluid flow increases with increasing the mass fraction of the microtube because the dimensions of the microtube are smaller than the microchannel, creating a greater pressure drop. This pressure drop leads to an increase in pumping capacity. Increasing the nominal Re of the system increases the flow rate and as a result, increases its pumping power. However, the relationship between the diameter of the microtube and the pumping power is inverse. With increasing the diameter of the microtube, its resistance to flow decreases, and as a result, the pressure drop and the pumping power decrease. In Fig. 20, the cross symbols show the closest results to direct numerical modeling of the micro MCHS and confirm the good accuracy of estimating response surfaces. It should be noted that in Fig. 20 a, there is an upward behavior at Re = 150. The very small changes in pressure drop due to the change in diameter, compared to the higher nominal Re, cause the diagrams to show the response surfaces to exhibit such behavior.

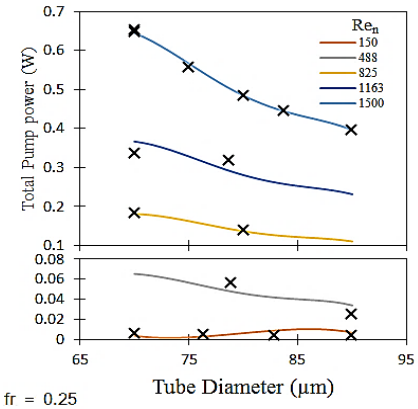

(a)

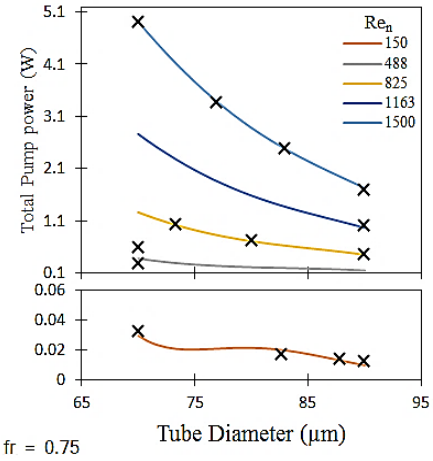

(b)

Fig. 20. Pumping power consumption in terms of nominal Re and diameter of microtube for different mass fractions

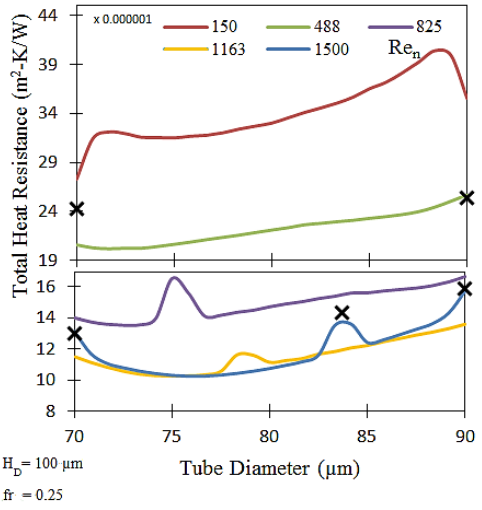

(a)

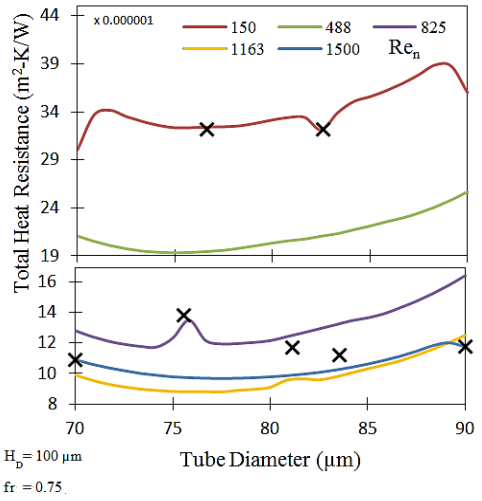

(b)

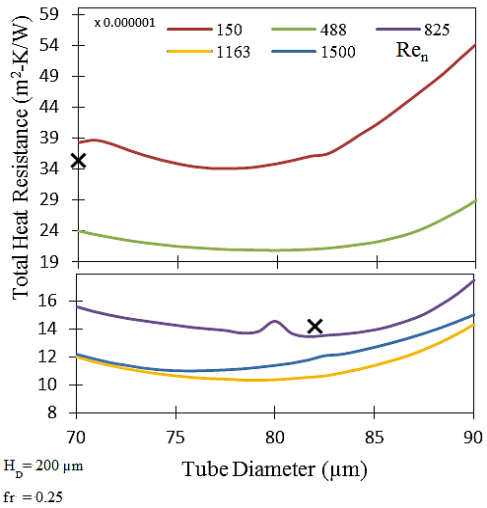

(c)

Fig. 21. Total thermal resistance in terms of microtube diameter, Re, mass fraction of flow, and microtube distance from the bottom.

Fig. 21 shows the thermal resistance of the system, which is plotted for five values of nominal Re in terms of microtube diameter. In Fig. 21 a, the mass fraction of the microtube flow rate is 0.25 and in Fig. 21 b, it is 0.75. Also, in Fig.

21 a, the height of the microtube from the bottom is 100 micrometers and in Fig. 21 c, is 200 micrometers. Comparing Figs. 21 a and b show that the effect of the mass flow rate of the microtube is dependent on Re. The higher Re, the greater the mass fraction. The reason can be attributed to the increase in heat capacity of the flow due to the increase in flow rate. At low values of Re, the flow velocity is low that causing the heat to be absorbed by the entire volume of the fluid. Due to the low heat capacity of the system, this volume of fluid absorbs its energy very quickly. As a result, increasing the flow in the microtube does not affect the absorption of the heat. However, at high flow rates where the heat capacity is high, the flow velocity makes it impossible to increase the heat capacity of the fluid. Thus, as the flow rate in the microtube increases, the access of the fluid to the hot surfaces increases, which will reduce the thermal resistance. For a better analysis of this issue, a case study of different samples should be done in the relevant section. The parameter of the distance of the microtube from the bottom is the same as the mass fraction flow in the microtube and has a greater effect on the flow with a high Re. It is observed that increasing this distance increases the thermal resistance of the system. Fig. 22 shows the average CPU surface temperature in terms of the nominal Re. This figure shows that as Re increases, the CPU surface temperature decreases due to the increase in flow rate and the heat capacity of the system. This figure does not show a fixed and linear behavior to investigate the effect of the diameter of the microtube as well as its distance from the CPU surface. It indicates that there is a minimum point for the minimum CPU surface temperature based on the diameter and the distance from the CPU surface.

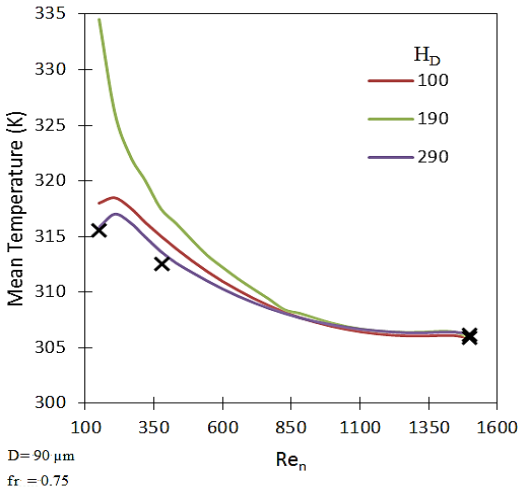

(a)

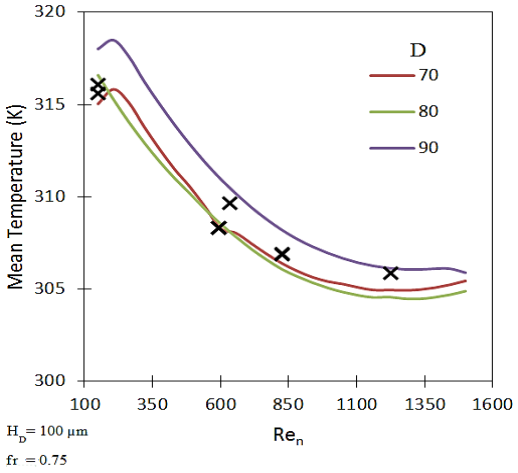

(b)

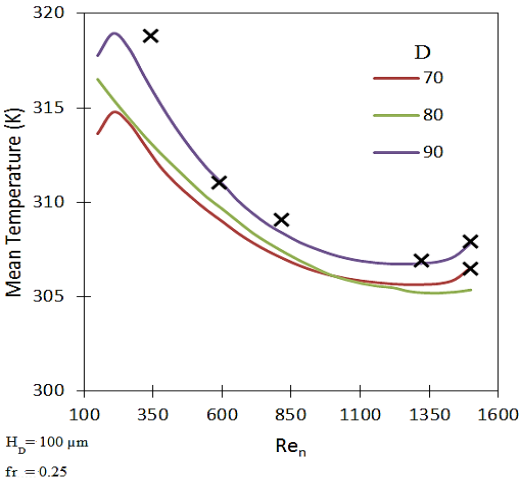

(c)

Fig. 22. CPU surface average temperature in terms of nominal Re.

Fig. 23 shows the total sgen in terms of the mass flow ratio of the microtube at different diameters for two different values of Re. Fig. 23a states that at low flow rates, sgen trend is unclear. The intersection of the lines of the figure shows the potential of this parameter for optimization. Fig. 23 b shows that at high flow rates, the amount of sgen increases with increasing mass flow fraction, which is due to the sharp increase in pressure drop due to an increase in the flow in the microtube. This figure also shows that the decrease in microtube diameter is nonlinearly related to the increase in sgen.

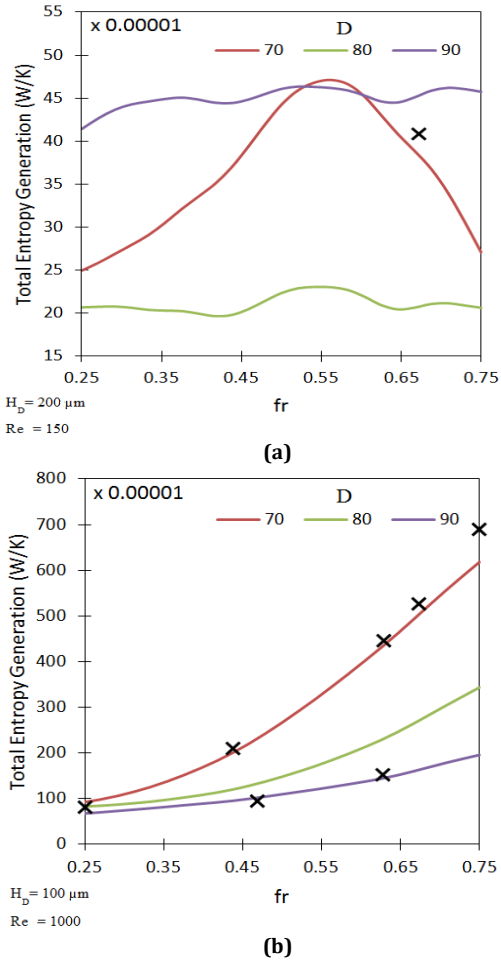

Fig. 23. Total sgen in terms of mass flow rate.

5. Conclusions

In the present study, biologically synthesized silver/water-ethylene glycol 50% nanofluid in a wavy MCHS was used. Numerical simulation and RSM were used to study the effect of adding microtube on the performance of microchannel MCHS. In this paper, after performing several simulations, the effect of total flow rate, the ratio of microchannel flow rate to microtube flow rate, location, and diameter of microtube on the response surface, including hydrodynamic parameters, thermal parameters, and sgen are investigated.

The main findings of the numerical modeling section of this research are as follows:

1- An enhancement of ϕ and Re lead to increasing h and improvement in the temperature uniformity of the CPU surface, Also the creation of microtubes due to the increase of heat transfer surface and decrease of thermal resistance in remote areas of the processor has caused a more uniform distribution in the surface temperature of the processor

2- Pumping power is reduced and is enhanced with ϕ and Re, respectively, which is more evident in the case without microtube

3- PEC investigation of silver/water-ethylene glycol 50% nanofluid demonstrates that the addition of nanofluid does not have the same effect for different cases.

In the continuation of the present study, the relationship between variables is determined by using the nonparametric regression model. This study aims to reach response surfaces with minimum error. Therefore, the accuracy of response surfaces was analyzed by performing new numerical simulations, and results of the accuracy of response surfaces about hydrodynamic parameters of the MCHS included pressure drop in microchannel and microtube, and pumping power is presented and very good accuracy of the results of the response surfaces for estimating the pressure drop of the models was presented.

Examination of the accuracy of the results of the response surfaces for the thermal parameters relative to the modeling values revealed that:

4- Response surfaces for estimating the maximum temperature of CPU surface in the worst cases have an error of less than 5% and the average temperature estimation of this surface has a maximum error of 3%, and therefore this response surface is a good estimate for these parameters.

5- The results of the accuracy of the response surface The temperature uniformity parameter on the CPU surface shows an error of 20% and as a result, this response surface is not a good estimate for this parameter.

6- It was found that the accuracy of the response surfaces for estimating the thermal resistance provides an acceptable estimate.

Then, from the accuracy diagrams of estimating the parameters related to entropy, it was found that estimating the response surfaces for the total sgen in the model has very acceptable accuracy. But these response surfaces work much better for the frictional sgen in the separate estimation of frictional and thermal entropy.

Finally, according to the obtained response surfaces, based on the defined input parameters including system flow, microtube to microchannel flow ratio, microtube diameter, and microtube distance from the MCHS surface, the MCHS behavior was analyzed. Among the results of this section is that:

7- Pumping power is a hydrodynamic parameter and the distance of the microtube from the bottom of the MCHS does not affect it. But changing the other three parameters, namely mass fraction, nominal Re, and microtube diameter, changes the pumping power.

8- The mass fraction of the flow rate of the microtube is directly related to the increase of the pumping power and with the increase this, the pumping power increased.

Graphs of total thermal resistance in terms of microtube diameter, nominal Re, mass fraction of flow, and microtube distance from the floor of MCHS show that:

9- The mass flow rate of the microtube depends on the Re of fluid flow; the higher Re, the greater the mass fraction. The reason for this can be considered as the increase in the thermal capacity of the flow due to the increase in flow

10- The parameter of the distance of the microtube from the floor is the same as the fraction of the mass flow rate of the microtube and has a greater effect on the current with the high nominal Re, but it was observed that increasing the distance increases the thermal resistance of the system.

Also, the graph of total sgen in terms of input parameters showed that:

11- At low flow rates of the system, sgen trend is unclear, at high flow rates, the amount of sgen increases with increasing mass flow fraction which is due to the sharp increase in pressure drop due to the high flow rate in the microtube.

Conflict of interest

The authors declare that they have no conflict of interest.

References

[1] Yahng JS, Jeoung SC, Choi DS, Cho D, Kim JH, Choi HM, Paik JS. 2005 Dec 1. Fabrication of microfluidic devices by using a femtosecond laser micromachining technique and μ-PIV studies on its fluid dynamics. Journal of the Korean Physical Society, 47(6), pp. 977-981.

[2] Tüdős AJ, Besselink GA, Schasfoort RB. 2001. Trends in miniaturized total analysis systems for point-of-care testing in clinical chemistry. Lab on a Chip, 1(2), pp.83-95.

[3] Tuckerman DB, Pease RF. 1981 May. High-performance heat sinking for VLSI. IEEE Electron device letters, 2(5), pp.126-129.

[4] Ho CJ, Wei LC, Li ZW. 2010 Feb 1. An experimental investigation of forced convective cooling performance of a microchannel heat sink with Al2O3/water nanofluid. Applied Thermal Engineering, 30(2-3), pp.96-103.

[5] Chen CH, Ding CY. 2011 Mar 1. Study on the thermal behavior and cooling performance of a nanofluid-cooled microchannel heat sink. International journal of thermal sciences, 50(3), pp.378-384.

[6] Vinodhan VL, Rajan KS. 2014 Oct 1. Computational analysis of new microchannel heat sink configurations. Energy Conversion and Management, 86, pp.595-604.

[7] Fani B, Kalteh M, Abbassi A. 2015 Jan 1. Investigating the effect of Brownian motion and viscous dissipation on the nanofluid heat transfer in a trapezoidal microchannel heat sink. Advanced Powder Technology;26(1), pp.83-90.

[8] Kalteh M, Abedinzadeh SS. 2018 Mar. Numerical investigation of MHD nanofluid forced convection in a microchannel using lattice Boltzmann method. Iranian Journal of Science and Technology, Transactions of Mechanical Engineering.;42(1), pp.23-34.

[9] Lin L, Zhao J, Lu G, Wang XD, Yan WM. 2017 Aug 1. Heat transfer enhancement in microchannel heat sink by wavy channel with changing wavelength/amplitude. International Journal of Thermal Sciences, 118, pp.423-434.

[10] Rostami, J., Abbassi, A., and Saffar-Avval, M., 2015. Optimization of Conjugate Heat Transfer in Wavy Walls Micro Channels. Applied Thermal Engineering, Vol. 82, pp. 318-328.

[11] Khorasanizadeh H, Sepehrnia M, Sadeghi R. 2017 Feb 10. Three dimensional investigations of inlet/outlet arrangements and nanofluid utilization effects on a triangular microchannel heat sink performance. Modares Mechanical Engineering, 16(12), pp.27-38.

[12] Ahmed HE, Ahmed MI, Seder IM, Salman BH. 2016 Oct 1. Experimental investigation for sequential triangular double-layered microchannel heat sink with nanofluids. International Communications in Heat and Mass Transfer,77, pp.104-115.

[13] Ghasemi SE, Ranjbar AA, Hosseini MJ. 2017 Mar 1. Thermal and hydrodynamic characteristics of water-based suspensions of Al2O3 nanoparticles in a novel minichannel heat sink. Journal of Molecular Liquids, 230, pp.550-556.

[14] Tafarroj MM, Mahian O, Kasaeian A, Sakamatapan K, Dalkilic AS, Wongwises S. 2017 Aug 1. Artificial neural network modeling of nanofluid flow in a microchannel heat sink using experimental data. International Communications in Heat and Mass Transfer, 86, pp.25-31.

[15] Ali HM, Arshad W. 2017 Mar 1. Effect of channel angle of pin-fin heat sink on heat transfer performance using water based graphene nanoplatelets nanofluids. International Journal of Heat and Mass Transfer, 106, pp. 465-472.

[16] Peyghambarzadeh, S., Hashemabadi, S., Chabi, A., and Salimi, M., 2014. Performance of Water Based CuO and Al2O3 Nanofluids in a Cu–Be Alloy Heat Sink with Rectangular Micro Channels, Energy Conversion and Management, Vol. 86, pp. 28-38.

[17] Hajialigol N, Fattahi A, Ahmadi MH, Qomi ME, Kakoli E. MHD, 2015 Jan 1. mixed convection and entropy generation in a 3-D microchannel using Al2O3–water nanofluid. Journal of the Taiwan Institute of Chemical Engineers, 46, pp.30-42.

[18] Wang CT, Hu YC. 2010 Dec. Mixing of liquids using obstacles in y-type microchannels. Journal of Applied Science and Engineering, 13(4), pp. 385-394.

[19] Sarlak A, Ahmadpour A, Hajmohammadi MR, 2019 Jan 25. Thermal design improvement of a double-layered microchannel heat sink by using multi-walled carbon nanotube (MWCNT) nanofluids with non-Newtonian viscosity. Applied Thermal Engineering, 147, pp.205-215.

[20] Hajmohammadi MR, Alipour P, Parsa H, 2018 Nov 1. Microfluidic effects on the heat transfer enhancement and optimal design of microchannels heat sinks. International Journal of Heat and Mass Transfer, 126, pp.808-815.

[21] Al-Rashed AA, Shahsavar A, Rasooli O, Moghimi MA, Karimipour A, Tran MD. 2019 May 1. Numerical assessment into the hydrothermal and entropy generation characteristics of biological water-silver nano-fluid in a wavy walled microchannel heat sink. International Communications in Heat and Mass Transfer, 104, pp.118-126.

[22] Azizi, Z., Alamdari, A., and Malayeri, M., 2015. Convective Heat Transfer of Cu–water Nanofluid in a Cylindrical Microchannel Heat Sink. Energy Conversion and Management, Vol. 101, pp. 515-524.

[23] Subasi A, Sahin B, Kaymaz I, 2016 Oct 1. Multi-objective optimization of a honeycomb heat sink using Response Surface Method. International Journal of Heat and Mass Transfer, 101, pp.295-302.

[24] Witek-Krowiak A, Chojnacka K, Podstawczyk D, Dawiec A, Pokomeda K. 2014 May 1. Application of response surface methodology and artificial neural network methods in modelling and optimization of biosorption process. Bioresource technology, 160, pp.150-160.

[25] Myers RH, Montgomery DC, Anderson-Cook CM. 2016 Jan 4. Response surface methodology: process and product optimization using designed experiments. John Wiley & Sons.

[26] Sarafraz MM, Hormozi FJ. 2015 Sep 1. Intensification of forced convection heat transfer using biological nanofluid in a double-pipe heat exchanger. Experimental Thermal and Fluid Science, 66, pp.279-289.

[27] Bejan A. 2016 Sep 19. Advanced engineering thermodynamics. John Wiley & Sons.

[28] Sui Y, Lee PS, Teo CJ. 2011 Dec 1. An experimental study of flow friction and heat transfer in wavy microchannels with rectangular cross section. International journal of thermal sciences, 50(12), pp.2473-2482.

[29] Myers RH, Montgomery DC, Anderson-Cook CM. 2016 Jan 4. Response surface methodology: process and product optimization using designed experiments. John Wiley & Sons.